water: an attempt to state the problem. *Bull. Geol. Soc. Am.* **62,** 1111.

Sagan, C. (1962). Structure of the lower atmosphere of Venus. *Icarus* **1,** 151.

Sagan, C., and Pollack, J. B. (1966). On the nature of the clouds and the origin of the surface temperature of Venus. *Astron. J.* **71,** 178.

Schmidt, A. (1953). Über das System Chlorwasserstoff/Wasser. *Chemie-Ing. Technol.* **25,** 455.

Spinrad, H. (1962). Spectroscopic temperature and pressure measurements in the Venus atmosphere. *Publ. Astron. Soc. Pacific* **74,** 187.

Spinrad, H., and Shawl, S. J. (1966). Water vapor on Venus—A confirmation. *Astrophys. J.* **146,** 328.

Suess, H. E. (1964). Remarks concerning the chemical composition of the atmosphere of Venus. *Z. Naturforsch.* **19a,** 84.

Suess, H. E., and Urey, H. C. (1956). Abund of the elements. *Rev. Mod. Phys.* **28,** 53

Toulmin, P., and Barton, P. B. (1964). A th dynamic study of pyrite and pyrrhotite *chim. Cosmochim. Acta* **28,** 641.

Urey, H. C. (1952). "The Planets." Yale Press, New Haven, Connecticut.

de Vaucouleurs, G., and Menzel, D. H. Results of the occultation of Regulus by July 7, 1959. *Nature* **188,** 28.

Walter, L. S. (1963). Experimental studie Bowen's decarbonation series: II: *P-T* variant equilibria of the reaction: Forsterite Calcite = Monticellite + Periclase + CO_2 *J. Sci.* **261,** 245.

Weeks, W. F. (1956). A thermochemical study equilibrium relations during metamorphis siliceous carbonate rocks. *J. Geol.* **64,** 245.

us 8, 457–471 (1968)

A Radar Study of the Lunar Crater Tycho at 3.8-cm and 70-cm Wavelengths

G. H. PETTENGILL

Lincoln Laboratory,[1] Massachusetts Institute of Technology, Lexington, Massachusetts

AND

T. W. THOMPSON

Cornell-Sydney University Astronomy Center, Arecibo Ionospheric Observatory[2]
Arecibo, Puerto Rico

Communicated by Zdeněk Kopal

Received October 26, 1967

Maps of the intensity distribution of radar echoes at 3.8- and 70-cm wavelengths from the lunar surface are presented for the region surrounding the crater Tycho. Surface resolution at 3.8 cm was between 1 and 2 km and at 70 cm between 7 and 10 km. The average scattering enhancement for Tycho at 3.8 cm was found to be 2.0 ± 0.3 when observed in the polarized mode (signals received using a sense of circular polarization orthogonal to that transmitted). At 70 cm, average enhancements of 5.0 ± 1.0 and 15 ± 2 in the polarized and depolarized modes, respectively, were observed. Using assumptions derived from earlier observations, that 15% and 6% of the average lunar surface at wavelengths of 3.8 and 70 cm, respectively, acts as a diffuse scatterer, we find from our observations that approximately 80% of the interior surface of Tycho scatters diffusely at these wavelengths. Modulation of the intensity distribution associated with localized crater slopes is also observed.

I. Introduction

The crater Tycho has long been known a prominent feature of the lunar surface, rticularly at full moon when its extensive y system may be seen to cover a large rtion of the visible disk. The crater itself a diameter of about 85 km from rim to m and by any criterion ranks as one of e youngest features of the lunar landape. To provide a reference for later dission, an Earth-based photograph of the ater is given in Fig. 1. Here, as in the later figures, north is toward the bottom and astronautic west is to the right.

Observations of the Moon at infrared wavelengths under conditions of both eclipse and full solar illumination (Shorthill *et al.,* 1960; Saari and Shorthill, 1963; Salisbury and Hunt, 1967) have shown Tycho—as well as other young craters—to possess a significantly higher surface thermal conductivity than their environs. These findings may be explained by a combination of increased surface roughness and density, although it is generally felt that the latter is more important in explaining the infrared observations.

A method of localizing the distribution of radio scattering across the lunar surface, using coherent analysis of radar echoes,

---

Operated with support from the U. S. National onautics and Space Administration under Conct NSR 22-009-(106).

Operated with support from the U. S. National nautics and Space Administration under NGR 33-010-024.

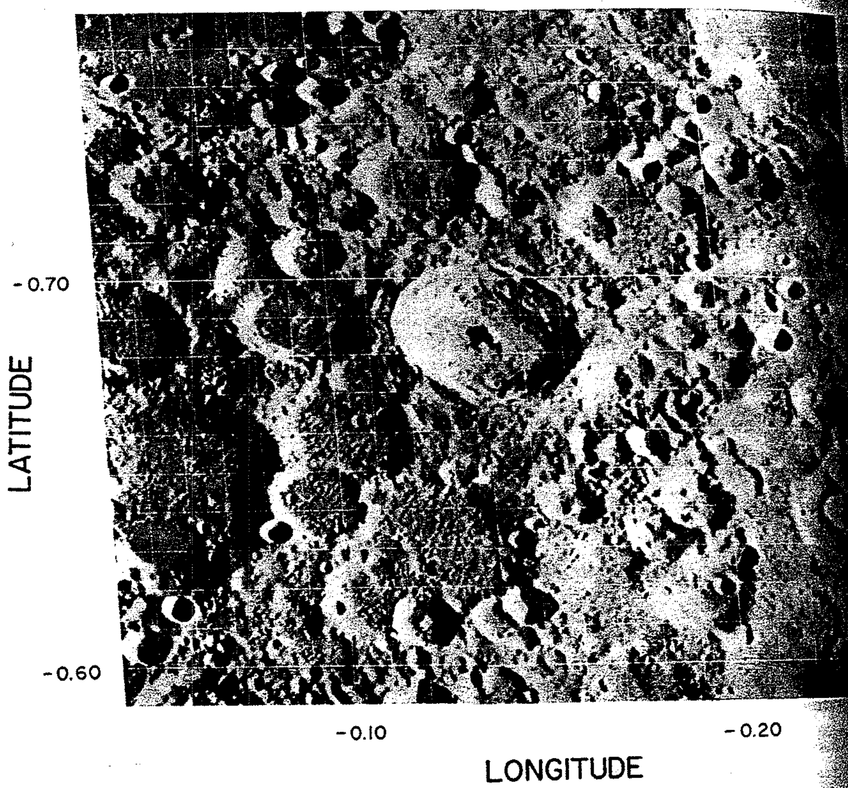

FIG. 1. Earth-based photograph of the region surrounding the lunar crater Tycho. Coordinates are orthographic projection with units of lunar radius. (Taken from "The Orthographic Atlas of the Mo G. P. Kuiper, ed., Univ. Ariz. Press, 1960.)

was first proposed by Green (1960). Pettengill (1960) showed that this technique, called delay-Doppler mapping, could be successfully applied to the Moon. Somewhat later, Pettengill and Henry (1962) were able to identify a region of particularly strong radar reflection at a wavelength of 68 cm as associated with the crater Tycho. Although the crater was not fully resolved, measurements in both the polarized and depolarized receiving modes were compared and it was concluded that wavelength-sized irregularities were the primary cause of the enhancement observed in the vicinity of Tycho. (In this paper, the polarized receiving mode refers to a receiving configuration which uses a sense of circular polarization orthogonal to transmitted; depolarized refers to the of the same sense.)

Thompson and Dyce (1966), using de Doppler radar techniques at 70-cm wa length, succeeded in resolving the Tycho and confirmed the earlier findings. With a resolution of about 25 they found that the scattering enhance was largely confined to the interior of crater. Comparison of measurements in the polarized and depolarized recei modes showed that the observed enha ment could be attributed entirely to creased roughness. In addition, a showing a twofold increase in refle power was noted which extended app

tely 100 km beyond the rim in all directions except to the south. Hagfors *et al.* 965) have also noted a high degree of olarization associated with radar echoes m Tycho at 23-cm wavelength.

In the present paper we report radar ervations of Tycho made with surface olutions of between 1 and 2 km at a velength of 3.8 cm and between 7 and 10 at a wavelength of 70 cm.

II. Procedures

The radar observations at 70 cm were rried out at the Arecibo Ionospheric servatory in Puerto Rico, operated by rnell University. The measurements at cm were taken using the Haystack crowave Facility in Massachusetts, opted by the Lincoln Laboratory of M.I.T. e radar operating characteristics for se observations are listed in Table I. nce the methods of data taking at both s were nearly identical, a single description is given. Where quantities differ, the lue applying at 70 cm is given first folwed by that for 3.8 cm in parentheses. nce the two-way, half-power antenna mwidth was only 7 (3) arcmin—a small fraction of the angle subtended by the lunar disk—it was important to direct the antenna at all times precisely at the crater Tycho. This was accomplished to an accuracy of about 1 (0.25) arcmin with the aid of a continuously operating digital computer.

The radar pulse length, sequence timing, and frequency were derived from a very precise standard whose absolute frequency was known to better than 1 (0.1) part in 10^{10} and whose short-term stability was at least 10 times better. During the observations, samples in digital form of the complex received waveform were recorded at 100 (200) positions in delay. These positions were accurately maintained relative to the lunar surface using calculations based on the lunar ephemeris. In the 3.8-cm observations 10 of these delay samples were reserved for a measure of the background noise and were placed well before the arrival of any lunar echo. (In the 70-cm observations, the background noise was estimated from a portion of the frequency spectrum known to contain no echo.) The remaining samples were approximately centered on the calculated delay corre-

TABLE I

Operating and Processing Parameters for the Radar Observations

	Arecibo	Haystack
Radar Location, latitude (geod.)	18°20′46″ N	42°37′24″ N
longitude	66°45′11″ W	71°29′19″ W
Operating frequency (MHz)	430	7840
wavelength	69.8	3.8
Antenna gain (db)	~56	66
Half-power, two-way beamwidth (arcmin)	7	3
Transmitted peak power (kw)	1000	200
Average power (w)	400	51/13
Polarization	Circular	Circular
Pulse width (μsec)	40	10/5
Interpulse interval (msec)	100	39/78
Receiving system temperature on Moon (°K)	500°	190°
Fine sampling interval (μsec)	40	10/5
Coherent processing interval (sec)	51.2	10/20
Spectral sample spacing (Hz)	0.02	0.10/0.05
Half-power spectral resolution (Hz)	0.017	0.09/0.04
Half-power delay resolution (μsec)	23	6/3
Date observations carried out (1967)	17 April	21 March
Duration of runs (min)	39	15/30
Number of coherent intervals summed	46	90

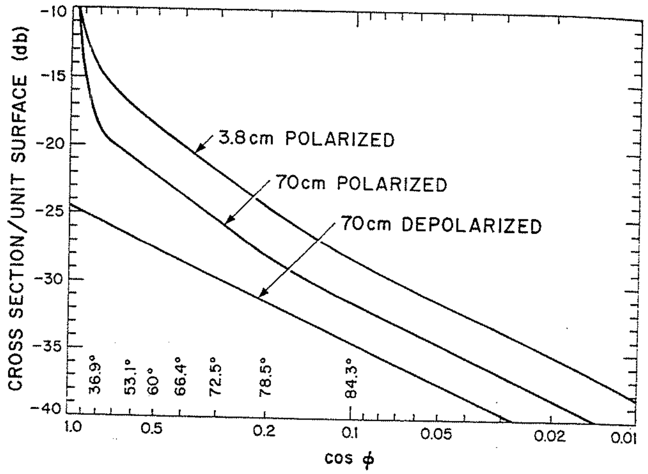

FIG. 2. Lunar scattering laws at 70-cm and 3.8-cm wavelengths. The abscissa has been made linea log cos φ, where φ is the angle of incidence to the mean lunar surface, in order to bring out the depende on cos φ of the scattering in the polarized mode at large, nearly grazing angles of incidence. The depolari scattering law at 70-cm wavelength varies quite accurately as cos φ. The ordinate is in terms of the speci radar cross section.

sponding to the center of the crater Tycho, and were spaced at intervals equal to the transmitted pulse length. Thus 100 (200) complex numbers were recorded for each interval following a transmitted pulse. The pulse responsible for a given observed echo, of course, would have been transmitted about 2.6 sec earlier. For the 70-cm observations, two modes of received polarization were sampled simultaneously using separate receivers. The transmitted pulse lengths, interpulse intervals, and other relevant parameters used for the runs reported here are listed in Table I. Circular senses of polarization were used for both transmission and reception, in order to obviate the effects at 70 cm of Faraday rotation in the ionosphere.

Following the recording of the data as described above, a Fourier analysis was carried out of the complex time series consisting of samples taken from consecutive interpulse intervals for each of the 100 (200) finely spaced delay positions. Exactly 512 (256) elements were used in each series (with uniform weighting), yielding the frequency resolution and spacing given in Table I. Successive series of this length were formed and analyzed throughout [illegible] duration of the run.

Subsequent to the Fourier analysis, tran formations were applied to the data [illegible] carry it from the delay-Doppler coordin system of the observing radar over [illegible] conventional selenographic system, as [illegible] scribed in detail by Thompson (1966 Since the coordinate transformation var significantly over the course of a [illegible] incoherently summed subgroups of the su cessive Fourier-processed series were chos so that for each subgroup a fixed trans formation sufficed to maintain an accurac commensurate with the resolution of [illegible] experiment. Finally the results of each sub group were added to obtain the maps re ported here. The total number of inco herently summed elements, which is 46 (90 here, determines the statistical significan of each cell in a map. The estimated fra tional standard deviation obtained in [illegible] way is approximately 0.15 (0.10).

In the mapping reduction a number [illegible] corrections were applied to the power dete mined from the radar returns. First, [illegible] mean background noise was subtrac from the data. Then a correction [illegible] pplied to compensate for the known ngular response of the antenna. Because f the rapid variation of echo power with elay it was necessary to normalize the ata in delay against the mean lunar scattering laws (Fig. 2), in order to distinguish he local variations from the mean behavior f the surface. Finally, the intensities were ivided by the Jacobian of the appropriate ansformation in order to normalize them o unit area on the lunar surface. The rmalizations for scattering law and area were done assuming the lunar surface to be a sphere of radius 1738 km and thus did not correct for the effects of inclinations with respect to the local horizontal. In the mapping, the corrected radar data were transformed to lunar surface coordinates, using the lunar ephemeris. In this paper we have chosen an orthographic projection aligned on the lunar equator and first meridian (see Kuiper, 1960). The unit of this Cartesian system is the mean lunar radius.

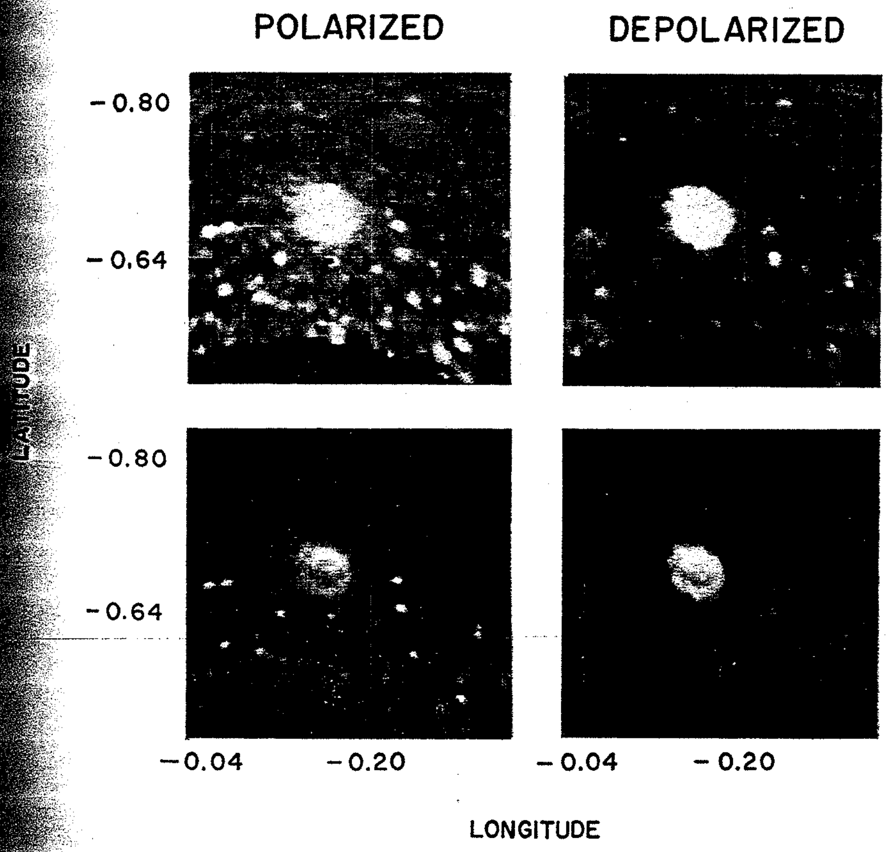

IG. 3. Radar maps of the region surrounding Tycho taken at a wavelength of 70 cm. Circular polarization transmitted and both senses of circular received. The left-hand pair of maps (polarized mode) were en using a received polarization orthogonal to that transmitted. The right-hand pair (depolarized mode) received in the same sense of circular polarization as that transmitted. Surface resolution here was 7 km ongitude and 10 km in latitude, or about one-tenth the diameter of Tycho. Because of the large dynamic e of the echoes, two levels of brightness (top and bottom) are shown for each map.

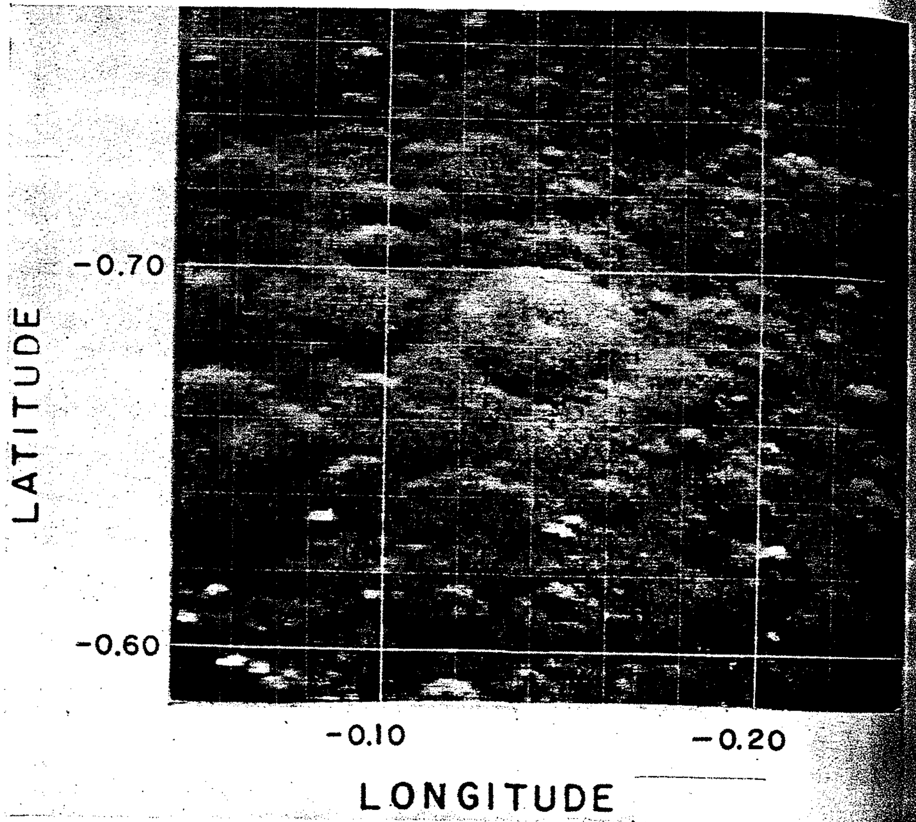

FIG. 4. Radar map of the region surrounding Tycho using circular polarization at a wavelength of 3.8 cm in the polarized mode. Surface resolution is about 2 km.

III. OBSERVATIONS

The output derived from a given radar observation represents a considerable quantity of data: between 10^4 and 10^5 values of intensity constitute a typical map. In order to present these data in a meaningful way, two methods have been chosen. The first of these writes a raster on an oscilloscope with the intensity at each point proportional to the localized enhancement. Photographs of this display thus provide an overview of the data in cartographic form, and are very useful for locating regions of atypical behavior. A drawback is the limited dynamic range available for displaying intensity and the difficulty in recovering data from the maps with adequate numerical accuracy. A second method which meets the latter objection is to draw a family of intensity profiles. It is obvious that the second method will be limited to regions of special interest.

The results of a radar observation at 70-cm wavelength in both senses of circular polarization are shown in Fig. 3. The dark sector at the bottom of the maps represents an area which lay outside the radar observations. Because of the large dynamic range exhibited by the surface reflectivity at 70 cm, particularly in the depolarized receiving mode, two levels of display exposure are given (top and bottom). It is immediately apparent that the contrast between the regions of localized enhancement and the general background is substantially greater in the depolarized mode. The enhancement associated with Tycho, although concentrated primarily inside the crater, appears to extend outside to a distance of as much as a crater radius beyond the rim.

In addition to Tycho, the prominent feature near the center, many other craters may be located. Among the largest of these is Longomontanus (—0.23, —0.76) in the upper right, with an enhancement which is visible in both polarizations but which is not nearly so great as for Tycho. Most of the features visible in Fig. 3 can readily be identified with craters seen in Fig. 1. A suggestion of ray structure from Tycho fanning out to the north (bottom of Fig. 3) may be seen, particularly in the polarized mode. This ray structure is visible in Earth-based optical photographs made at full moon, but is noticeably absent from Fig. 1. Optical photographs also show a variation in the azimuthal distribution of rays, but in the optical case this is less confined in azimuth and centered more to the east than is indicated by radar.

The results of two radar observations at 3.8-cm wavelength are shown in Figs. 4 and 5. The chief difference between the

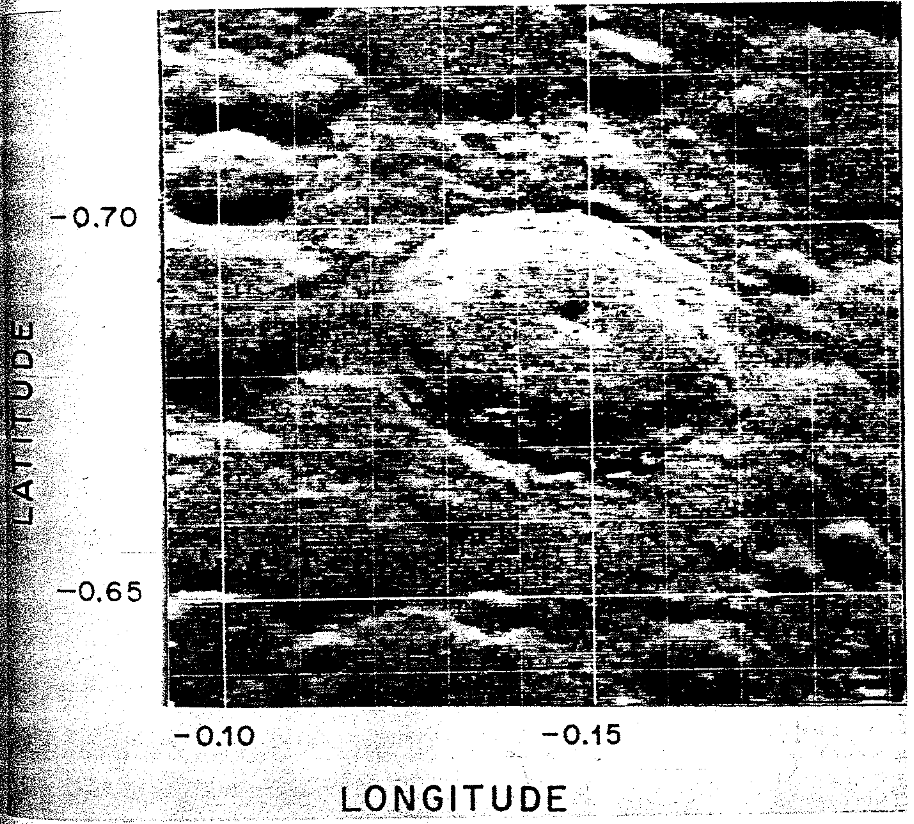

FIG. 5. Radar map of Tycho at 3.8-cm wavelength using circular polarization in the polarized mode. Surface resolution is about 1 km. The slight displacements in the positions of features as compared to Fig. 1 are related to inaccuracies in the lunar orbit currently available.

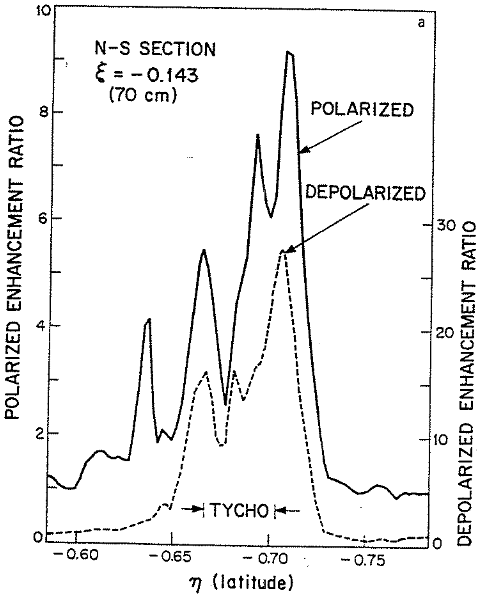

Fig. 6a

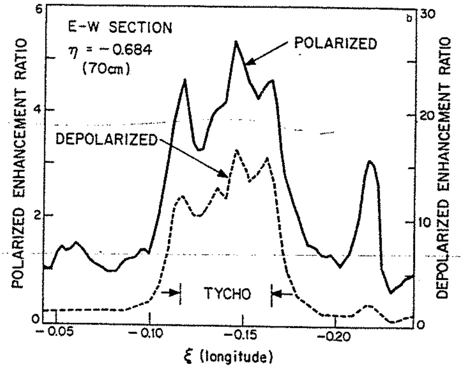

Fig. 6b

Fig. 6. Profiles of echo enhancement vs. position through the center of Tycho drawn from the data shown in Fig. 3 (70 cm). (a) Profile in latitude (north–south); (b) profile in longitude (east–west). Data from maps in both the polarized and depolarized modes are shown (read the polarized curve from the left scale, depolarized from the right), and have been normalized with respect to the mean lunar scattering law. The relative intensities of echoes in the two polarization modes have been approximately preserved.

two sets of observations lies in the twofold improvement in resolution (but reduced area of coverage) of Fig. 5. Only the polarized receiving mode was available in the 3.8-cm studies. Again, small gaps in the upper right and lower left of these figures represent areas where radar data were missing because of the finite delay sampling interval available.

The most immediately striking feature of the 3.8-cm observations is their resemblance to the optical photograph shown in Fig. 1. Despite the similarity in appearance, it should be remembered that the radar measurements were made with a full-moon type of illumination without shadowing, while Fig. 1 highlights the lunar slopes using the shadows cast by oblique sunlight. Thus, although it is the slopes that are primarily responsible for the observed intensity modulation in both cases, the detailed mechanism involved is different.

Comparing now the radar observations at the two wavelengths, the most important factor which appears to modulate the intensity of the 3.8-cm echoes seen in Figs. 4 and 5 is the slope with respect to the local horizontal of the region under observation. This factor is also present at 70 cm, as seen in Fig. 3, but is partly masked by the variations in backscattering resulting from surface roughness, which appear to be much larger than at 3.8-cm. The effect of tilting a resolved region of the lunar surface so as to lie more nearly normal to the radar direction is to increase its backscattering efficiency (see Fig. 2). If the region were typical of the average lunar surface this increase could be related to the tilt angle through the known lunar scattering law. But, of course, many of the craters seen by radar probably have atypical surface roughness as well as atypical small-scale slope distributions. However, if the crater profiles are known from optical shadow measurements, it should be possible to build up a family of such crater scattering laws from sufficiently fine-grained radar data. These, in turn, might prove to be correlated with relative surface roughness (determined independently from depolarized mode observations) at one or more wavelengths, and could be used to deduce slopes for those craters where optical shadow reductions were not available.

A more quantitative presentation of the enhancement associated with Tycho is given by the intensity profiles of Figs. 6 and 7. Figure 6 is derived from the 70-cm data of Fig. 3, and Fig. 7 from the 3.8-cm data of Fig. 4. The (a) portion of each figure represents the intensity profile along a plane parallel to the lunar polar axis which passes through the approximate center of Tycho. Similarly (b) in each figure represents the profile through the center of Tycho along a plane parallel to the lunar equator. Each plane is characterized by the coordinate given in the figure. The intensity has been normalized so that unity corresponds to the average lunar scattering at the appropriate delay and has been plotted as an enhancement ratio. In Fig. 6, where both modes of polarization are shown, the polarized data should be

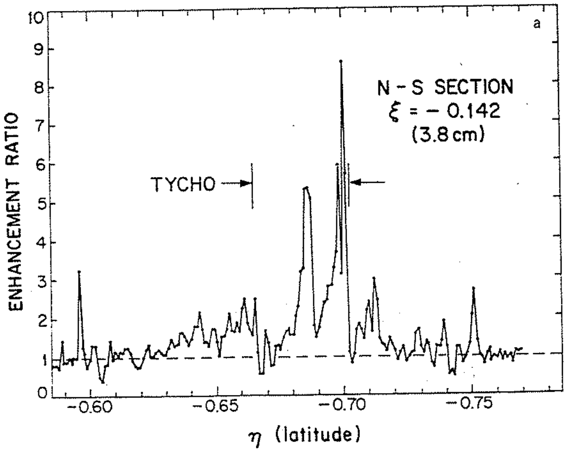

Fig. 7a

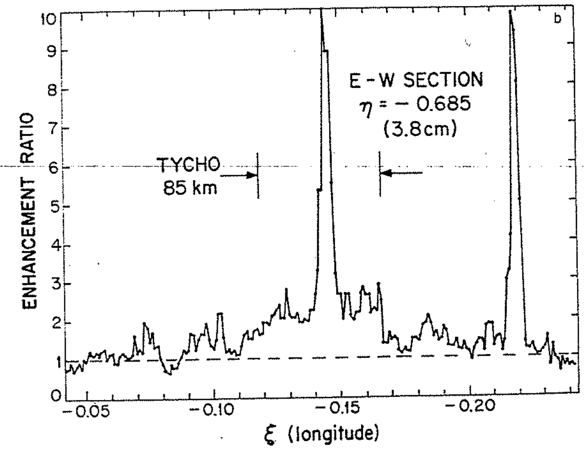

Fig. 7b

Fig. 7. Profiles of echo enhancement vs. position through the center of Tycho drawn from the data shown in Fig. 4 (3.8 cm). (a) Profile in latitude (north–south); (b) profile in longitude (east–west). Only data in the polarized mode were available. Note that the intensity peak near the center of Tycho is not located precisely at the intersection of the two profiles.

read from the left-hand ordinate and the depolarized from the right. The relationship between the absolute levels of scattering in the two polarizations has been preserved; thus, it may be seen that the power in the depolarized mode never exceeds that in the polarized (as it should not for any physically likely surface).

Since Tycho lies nearly due south of the center of the visible lunar disk, the north–south section maximizes the variation in the projection of the crater slopes with respect to the radar direction. The corresponding effect on the radar scattering can readily be seen in Figs. 6(a) and 7(a). Peaks associated with other craters may also be seen. Sasserides H, which is prominent in Fig. 6(a) at longitude −0.636, does not appear in Fig. 7(a) primarily because the section passes just to the east of the crater rim and the higher resolution of the 3.8-cm observations excludes its contribution. Note the relatively greater enhancement in the polarized mode as compared to the depolarized mode for this feature, indicating that the enhancement results primarily from a suitably aligned, specularly reflecting feature. In the case of Tycho, the reverse is true, that is, the enhancement is relatively greater in the depolarized component. Note also the contributions in both Figs. 6(a) and 7(a) associated with the central peak of Tycho. These differ slightly between the figures, again because of the difference in resolution and because the section of Fig. 7(a) passes slightly to the east of the peak. The higher resolution of Fig. 7(a) also appears to distinguish two radially separated sloping regions on both the north and south walls of the crater, presumably associated with slumping. This latter effect is even more clearly noted in Fig. 5.

As expected, Figs. 6(b) and 7(b), which are sections in the east–west plane through the center of Tycho, show remarkably little slope modulation since the projection of the crater slopes in the direction of the radar remains approximately constant except in the vicinity of the central peak. From an average over sections taken at a number of positions across Tycho, one derives average enhancements of 5.0 ± 1.0 and 15 ± 2 in the polarized and depolarized modes, respectively, at 70 cm and of 2.0 ± 0.3 in the polarized mode at 3.8 cm. Both profiles given in Fig. 7, as well as Fig. 4, show that the enhanced reflectivity at 3.8 cm associated with Tycho extends significantly outside the rim to a distance of at least several crater radii. Although the enhancement inside the crater at 3.8 cm is not as intense as at 70 cm, its extent appears to be somewhat greater. An enhancement associated with the far wall of the crater Street H may be seen just south of latitude −0.75 in both Figs. 6(a) and 7(a). A substantial enhancement associated with the southern lip of the crater Wilhelm O may also be seen near longitude −0.218 in both Figs. 6(b) and 7(b).

IV. Discussion

Two types of mechanisms have been discussed which appear to influence the local scattering from the lunar surface. These are associated with (1) variations in the surface slope with respect to the local horizontal, and (2) variations in the local amount of wavelength-sized structure. A third effect might well result from variations in the intrinsic reflectivity of the surface related to density and composition, although no radar evidence has yet been offered which requires such variations. The specific reflectivity of the average lunar surface at normal incidence has been found to be close to 0.064 at both 70- and 3.8-cm wavelengths (Evans and Pettengill, 1963; Evans and Hagfors, 1964), but local variations in this average figure are hard to distinguish unambiguously from the first two effects mentioned above.

Figure 2 presents the scattering laws which are relevant to the interpretation of the data reported here. They are based on observations reported by Evans and Pettengill (1963) at 68 cm, and on recent measurements at 3.8 cm carried out using the Haystack Microwave Facility. The conversion to specific cross section is as reported by Hagfors (1967). The ordinate is plotted as radar cross section per unit surface area and assumes incoherence between the average echo power returned by resolved areas of the surface—a valid assumption in the present experiment. Thus, the units are dimensionless and are plotted as logarithmic power ratios (db). The abscissa has been chosen as linear in log cos φ, where φ is the angle of incidence to the local horizontal, for both the illuminating radiation and the observed scattering. In this way, the dependence of the laws on various powers of cos φ is apparent. From about $\varphi = 45°$ to $80°$ the polarized mode laws vary quite accurately as $\cos^{3/2}\varphi$ but beyond about 80° both laws change over to a direct dependence on cos φ. The depolarized 70-cm law behaves as cos φ throughout its range of angles. For reference, at normal incidence ($\varphi = 0°$) the 70-cm polarized law yields +4.3 db, and the 3.8-cm polarized law +0.8 db; they cross over at $\varphi = 15°$. The total power under the two polarized mode curves is approximately the same, reflecting the similarity in total radar cross section at the two wavelengths. The total cross section for the 70-cm depolarized mode, however, is only about 0.06 times that for the polarized mode at the same wavelength.

The interpretation given to these laws here is to assign all of the depolarized scattering to wavelength-sized irregularities. Following the argument of Evans and Hagfors (1966), we assume that these irregularities may be viewed as asymmetries (effectively dipoles) which resolve the incident circularly polarized radiation into linear components of random phase. Thus they will return statistically equal amounts of power in both circular senses of received polarization. It is also expected that some fraction of the polarized mode scattering at large angles of incidence would arise from a component of the small-scale surface elements which exhibits symmetry around the direction of observation. From a consideration of the scattering laws in the two modes Evans and Hagfors (1966) found about equal amounts of small-scale symmetric and asymmetric scatterers distributed over the average lunar surface. It is perhaps dangerous to assume that these are necessarily wavelength-sized. Although they certainly cannot be a great deal smaller than the wavelength, they could in principle be larger. In fact, from the gradual increase in the amount of grazing angle ("diffuse") scattering as the wavelength is shortened (see, for example, Evans and Hagfors, 1964) it is tempting to conclude that the effect of surface roughness is to a certain extent cumulative, with an increasing fraction of the surface being covered as the lower size bound is reduced. In the optical limit, of course, we see a uniformly bright full moon (the optical backscattering law is known to vary approximately as cos φ).

From numerical integration of the curves shown in Fig. 2 it can be derived that approximately 12% of the total scattered power at 70-cm wavelength and approximately 25% at 3.8 cm is contained in the component which varies as cos φ and is, therefore, presumably associated with scattering by small-scale surface irregularities. This fraction is smaller than that quoted for the diffuse component by other workers because we have excluded here the $\cos^{3/2}\varphi$ component. In order to relate this fraction of power to the actual fraction of the lunar surface which is covered with these irregularities, it is necessary to know the directivity of the backscattering associated with the reflection mechanism. As is discussed more fully by Evans and Pettengill (1963), and by Evans and Hagfors (1964), this directivity cannot be firmly established unless the complete behavior of the scattering law is known for all directions of scattering. In the radar case, where only Earth-based observations have so far been feasible, this complete determination has not been possible. For the optical case, however, the Lommel-Seeliger law has been investigated for the more general case, since the illumination provided by the Sun can be observed over the full range of phase angles. In this case, the directivity can be shown to be approximately 2, and we have, therefore, assumed this value for the radar data as well, since the backscattered dependence of this component is observed to be similar at both radar and optical wavelengths.

Letting P_s represent the integrated power returned by the smooth (or quasi-specular) component of the average lunar surface, and P_r the power returned by the rough component, we may write the following ratio for the scattering observed in the polarized mode

$$P_r/P_s = g_r\chi_0/g_s(1 - \chi_0), \quad (1)$$

where g represents the directivity of the two laws in the backward scattering direction, and χ_0 the fraction of the average lunar surface to be associated with the rough component of scattering. Hagfors (1964) has shown that

$$g_s \cong 1 + \alpha^2, \quad (2)$$

where α is the r.m.s. surface slope, equal to approximately 0.1 at 68 cm and 0.2 at 3.6 cm. Assuming $g_r = 2$ and the integrated power ratios given above, we find that $\chi_0 \cong 0.057$ at 68 cm, and 0.146 at 3.6 cm. Implicit in this derivation, of course, is the assumption that the reflectivity of both components is the same. If the rough component of scattering is caused primarily by the "boulders" seen in the Surveyor spacecraft photographs (see discussion by Hagfors, 1967), then we might expect the reflectivity associated with these presumably denser objects to be larger than that of the more porous average lunar surface. This increase is by no means certain, but if present it will serve to reduce the fractions obtained above. In any event, it seems unlikely that the reflectivity would rise much above that for dry solid terrestrial rocks—about a factor of 2 greater than for the smooth portions of the lunar surface.

Since we have postulated that the depolarized scattering results entirely from the rough component of the surface, an enhancement in this mode such as is observed for Tycho requires a corresponding, proportional increase in the local roughness of the surface. This relationship, normalized to unity at $\chi_0 = 0.057$ for 68-cm wavelength is shown in Fig. 8, together with the depolarized enhancement for Tycho, which is observed to be 15. The corresponding fraction of the surface of Tycho which is required to be rough at a scale of approximately 70 cm is 0.85. This fraction would be reduced, of course, in proportion to any reduction which might later be found necessary in the fraction of average surface roughness.

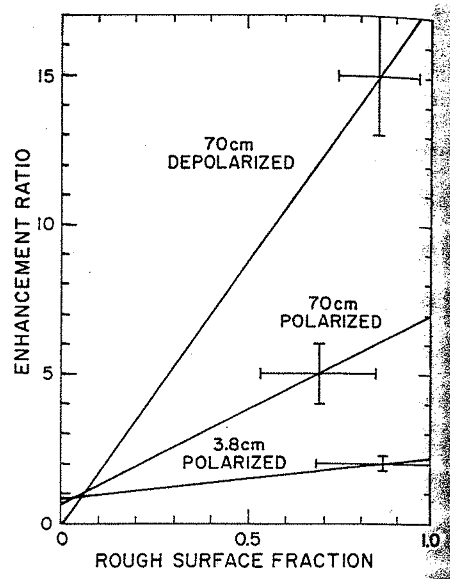

FIG. 8. Plot of the enhancement ratio to be expected for craters in the vicinity of Tycho as a function of their fractional surface roughness. Mean values of roughness for the lunar surface of 0.057 at 70-cm wavelength and 0.146 at 3.8 cm have been assumed.

In the polarized case, the enhancement is complicated by the presence of the smooth scattering component which must be reduced in proportion to (1-χ). Thus we may write for the enhancement at a particular angle of incidence φ, and for a local surface roughness fraction χ

$$\frac{(\chi/\chi_0)P_r(\varphi) + (1 - \chi)/(1 - \chi_0)P_s(\varphi)}{P_r(\varphi) + P_s(\varphi)}, \quad (3)$$

where $P_r(\varphi)$ and $P_s(\varphi)$ are the scattering laws for the rough and smooth components, respectively, and may be obtained for a given φ from the data shown in Fig. 2. The rough component is assumed to vary as cos φ in agreement with the depolarized law and is obtained by matching to the cos φ "tail" of the two polarized curves. At $\varphi \cong 37°$ (the approximate value for Tycho in both sets of observations reported here), $P_r(\varphi)/[P_r(\varphi) + P_s(\varphi)] = 0.40$ at 70 cm and 0.32 at 3.8 cm. Again assuming values for χ_0 as given above, the polarized enhancement expected in these observations is given as a function of χ in Fig. 8. As may be seen from relation (3) and Fig. 2, the polarized enhancement for a given value of χ will vary significantly with φ, and in fact will become identically equal to unity for values of φ where

$$\frac{P_r(\varphi)}{P_s(\varphi)} = \frac{\chi_0}{1 - \chi_0}. \quad (4)$$

This degeneracy should occur at $\varphi = 17°$ for 70 cm, and $\varphi = 23°$ for 3.8 cm. In principle, at least, a measurement of these angles could serve as a direct measurement of χ_0 which is independent of the assumptions of surface reflectivity required above.

The polarized enhancements observed for Tycho are plotted in Fig. 8 for both wavelengths, and it is interesting that all three measurements are in fair agreement with $\chi = 0.8$. Underlying the polarized mode relationships shown in Fig. 8, of course, is the assumption that the smooth component of scattering, when normalized by $(1-\chi_0)/(1-\chi)$, is identical with that observed for the average lunar surface. Since Tycho is anomalous in its rough surface fraction, there may also be anomalies in the distribution of inclinations of quasi-smooth surface slopes. Because the surface roughness found here for Tycho is so large, however, small departures from average in the

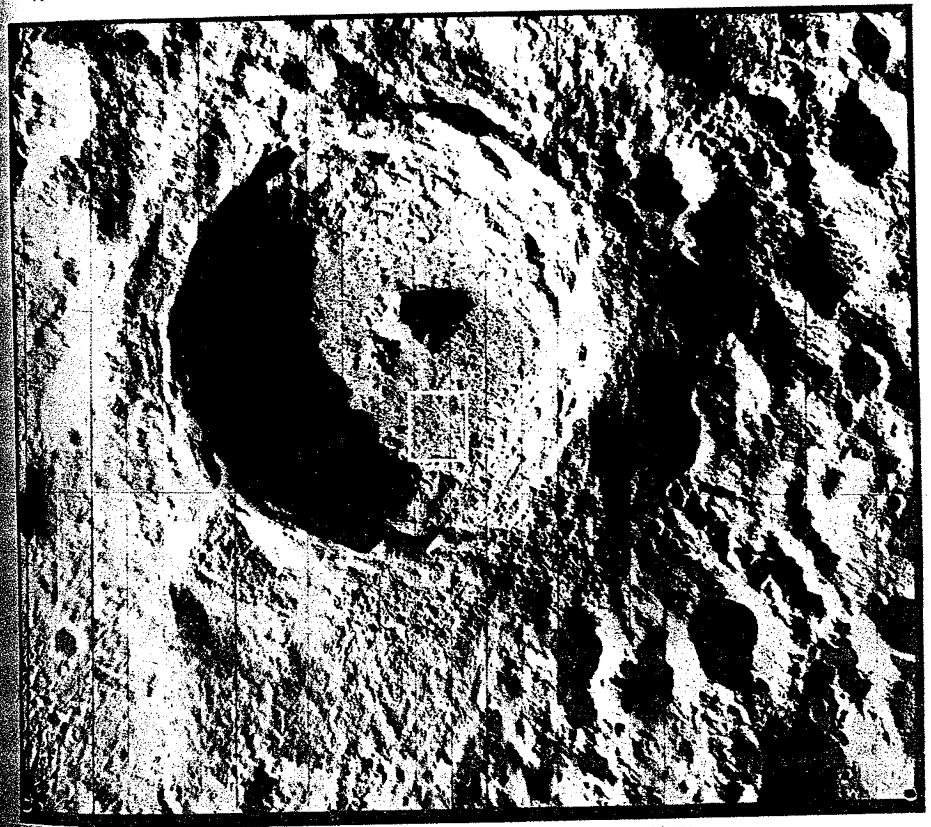

FIG. 9. Medium resolution aerial photograph of the lunar crater Tycho as obtained 15 August 1967 by Lunar Orbiter V (frame M-123). Courtesy of the National Aeronautics and Space Administration, taken from photo 67-H-1206. Area included in Fig. 10 is shown outlined by the rectangle.

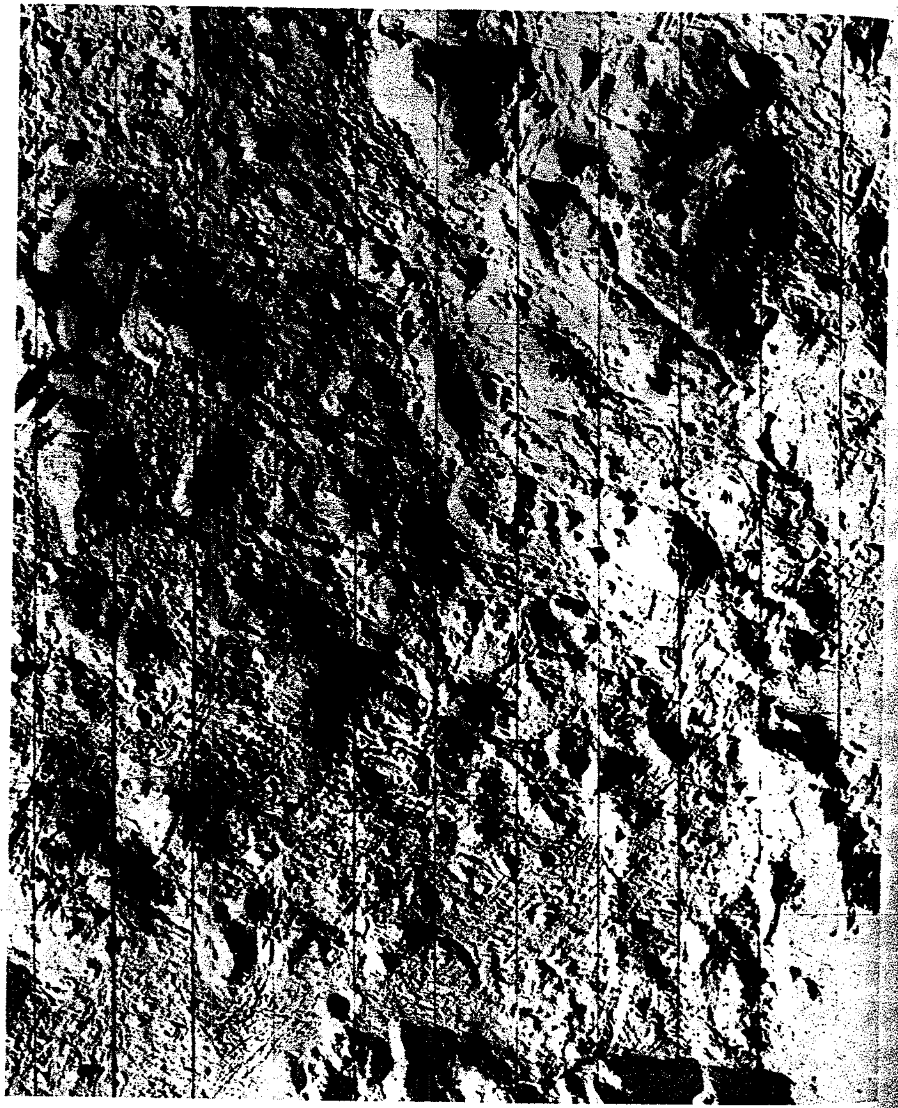

FIG. 10. High-resolution aerial photograph of the portion of the floor of Tycho outlined in Fig. 9. Taken by Lunar Orbiter V, 15 August 1967 simultaneously with Fig. 9. Area covered is roughly 11 by 13 km. Courtesy of the National Aeronautics and Space Administration.

smooth scattering law will not be important. A departure of this sort, nevertheless, may explain the slight discrepancy between the surface roughness determined in the two modes of 70-cm polarization.

Further evidence that the crater floor of Tycho is far rougher than the typical lunar surface has recently been obtained by the spacecraft Lunar Orbiter V. In Fig. 9 is shown a wide-angle overhead photograph of Tycho and in Fig. 10 a narrow-angle, high-resolution photograph of a region of the crater floor (outlined in Fig. 9). Both photographs were taken simultaneously on 15 August 1967. The resolution in Fig. 10 is better than 20 m and the extreme roughness of the surface may readily be seen. It would appear that the impact which created the crater, as well as subsequent flows and cooling, have created an extremely jagged surface which is rough on both a large and small scale. Since the same original conditions may be postulated for all other similarly large craters, the fact that Tycho now appears relatively anomalous requires the operation of a mechanism which "heals" the lunar surface, although this process must certainly go forward at a rate several orders of magnitude more slowly than those processes which modify the surface of the Earth.

In conclusion, observations of Tycho by radar and by direct photography have found the crater floor to possess a high degree of roughness (as compared to the average lunar surface) at scales ranging from a few cm up to tens of meters. Observations of the other craters using both polarized and depolarized modes are urged to see whether the enhancements found for Tycho may not be exceeded, for, if a rough-surface fraction in excess of unity is found under the assumptions used above, a local increase in surface density may be directly inferred.

ACKNOWLEDGMENTS

The enthusiastic support of the entire staff of the Arecibo and Haystack radar facilities in carrying out these observations is gratefully acknowledged. At Haystack, L. G. Kraft and R. P. Ingalls were directly responsible for the radar operation, R. Wells (of Adams Associates) for much of the programming, and J. F. MacLeod for direct assistance in the data reduction. At Arecibo, the assistance of H. Cabassa in preparation of several of the digital computer programs was invaluable. The use of high-speed, Cooley-Tukey algorithms in the Fourier processing was made possible at both facilities through the efforts of N. Brenner of Lincoln Laboratory.

We are indebted to the general support for the Haystack facility made available by the U. S. Air Force, as well as to continuing support for the Arecibo facility provided by the Advanced Research Projects Agency under contract with the U. S. Air Force Office of Scientific Research.

REFERENCES

EVANS, J. V., AND HAGFORS, T. (1964). On the interpretation of radar reflections from the Moon. *Icarus* **3**, 151–160.

EVANS, J. V., AND HAGFORS, T. (1966). Study of radio echoes from the moon at 23 cm wavelength. *J. Geophys. Res.* **71**, 4871–4889.

EVANS, J. V., AND PETTENGILL, G. H. (1963), The scattering behavior of the moon at wavelengths of 3.6, 68, and 784 cm. *J. Geophys. Res.* **68**, 423–447.

GREEN, P. E., Jr. (1960). Radar astronomy symposium report (R. L. Leadabrand, ed.). *J. Geophys. Res.* **65**, 1108–1115.

HAGFORS, T. (1964). Backscattering from an undulating surface with applications to radar returns from the moon. *J. Geophys. Res.* **69**, 3779–3784.

HAGFORS, T. (1967). A study of the depolarization of lunar radar echoes. *Radio Sci. (New Series)* **2**, 445–465.

HAGFORS, T., BROCKELMAN, R. A., DANFORTH, H. H., HANSON, L. B., AND HYDE, G. M. (1965). Tenuous surface layer on the moon: evidence derived from radar observations. *Science* **150**, 1153–1156.

KUIPER, G. P. (1960). "Orthographic Atlas of the Moon." Univ. of Arizona Press, Tucson, Arizona.

PETTENGILL, G. H. (1960). Measurements of lunar reflectivity using the Millstone Radar. *Proc. IRE* **48**, 933–934.

PETTENGILL, G. H., AND HENRY, J. C. (1962). Enhancement of radar reflectivity associated with the lunar crater Tycho. *J. Geophys. Res.* **67**, 4881–4885.

SAARI, J. M., AND SHORTHILL, R. W. (1963). Isotherms of crater regions on the illuminated and Eclipsed moon. *Icarus* **2**, 115–136.

SALISBURY, J. W., AND HUNT, G. R. (1967). Infrared images: implications for the lunar surface. *Icarus* **7**, 47–58.

SHORTHILL, R. W., BOROUGH, H. C., AND CONLEY, J. M. (1960). Enhanced lunar thermal radiation during a lunar eclipse. *Publ. Astron. Soc. Pacific* **72**, 481–485.

THOMPSON, T. W. (1966). A study of radar-scattering behavior of lunar craters at 70 cm. Thesis, Cornell Univ, Dept. of Electrical Engineering, Ithaca, New York.

THOMPSON, T. W., AND DYCE, R. B. (1966). Mapping of lunar radar reflectivity at 70 cm. *J. Geophys. Res.* **71**, 4843–4853.